Study of the corrosion resistance and *in vitro* biocompatibility of PVD TiCN-coated AISI 316 L austenitic stainless steel for orthopedic applications

R.A. Antunes [a],*, A.C.D. Rodas [b], N.B. Lima [b], O.Z. Higa [b], I. Costa [b]

[a] *Engineering, Modeling and Applied Social Sciences Center (CECS), Federal University of ABC (UFABC), CEP 09210-170, Santo André, SP, Brazil*
[b] *IPEN/CNEN-SP, Av. Prof. Lineu Prestes 2242, CEP 05508-900, São Paulo, SP, Brazil*

ARTICLE INFO

ABSTRACT

The aim of the present work was to study the corrosion resistance in Hanks' solution and the *in vitro* biocompatibility of a TiCN-coated AISI 316 L stainless steel. The electrochemical behavior was assessed using potentiodynamic polarization and electrochemical impedance spectroscopy. Cytotoxicity and genotoxicity tests were performed to evaluate the potential biocompatibility of the specimens. TiCN morphology was investigated using scanning electron microscopy (SEM). Bare 316 L specimens were also evaluated for comparison. The results showed that the film morphology strongly influences the electrochemical behavior of the coated underlying metal. TiCN-coated specimens presented neither cytotoxicity nor genotoxicity.

© 2010 Elsevier B.V. All rights reserved.

1. Introduction

The use of austenitic stainless steels for orthopedic applications is widespread due to a combination of good mechanical properties and easy fabrication at low cost [1]. However, it is well known that these materials are prone to localized corrosion in the body fluids [2]. Removed stainless steel implants often present signs of pitting or crevice corrosion. The combined effect of corrosion and fatigue may lead to implant failure. Furthermore, several authors report the undesirable influence of corrosion products leached to surrounding tissues in the vicinity of the implant device. This interaction may cause allergic or infectious reactions which, in turn, may lead, in ultimate cases, to the loosening of the biomedical device [3].

Different types of PVD hard ceramic coatings are frequently considered to overcome the drawbacks mentioned above. Titanium carbonitride (TiCN) for instance presents excellent wear resistance, high hardness, good thermal conductivity and high electric conductivity. Thus, TiCN films are employed as a protective layer in tool steels and semiconductors [4]. Good corrosion resistance is also reported in the literature [5]. Feng et al. [4] reported a decrease of up to three orders of magnitude for the corrosion current density of TiCN-coated AISI 304 stainless steel. Besides, its non cytotoxic character allied with mechanical and corrosion properties make it a very interesting material for biomedical applications. Recently, Serro et al. [6] reported an investigation on the suitability of TiCN coatings for the improve-

ment of the wear resistance of ultra high molecular weight polyethylene (UHMWPE) component of orthopaedic joint implants. In a previous study, the same group [7] reported that TiCN-coated 316 L stainless steel presented excellent wear resistance in ball-on-disk tests. Although the wear and fatigue behaviors of TiCN coatings are extensively studied [8–12] there is little information on the corrosion resistance of carbonitrided austenitic stainless steels in physiological solutions and on how the immersion in such environments affects the structure of the TiCN films. One of the few studies on the corrosion of TiCN as a biomaterial is due to Hollstein and Louda [13]. They have assessed the corrosion resistance of TiCN-coated stainless steel as a PVD protective layer on surgery instruments. The results pointed to a slow kinetics of the corrosion processes and a good biocompatibility of the PVD film.

It should be considered, though, that metal substrates under PVD coatings are prone to corrosion attack. The structure of these hard ceramic layers presents inherent defects such as pinholes, micro-cracks and macroparticles. According to Mattox [14], macroparticles are generated during the evaporation of the cathode in the vacuum evaporation PVD method. Small globules of the solid cathode are ejected as it vaporizes and deposit on the coating layer. Consequently, swollen regions are created during the deposition process which can generate small cavities. Thus, the defects on the PVD layer consist of preferential paths to the diffusion of aggressive species into the substrate underneath the protective coating. The metal on the base of the PVD film may, then, present localized corrosion [15–17].

The biocompatibility of coating materials is of great importance for a successful use in biomedical devices. *In vitro* cytotoxicity tests are recommended by the International Organization for Standardization

Table 1
Chemical composition of the 316 L stainless steel (mass percentage).

Element	C	Si	P	S	Cr	Mn	Cu	Ni	Mo	N	Fe
Mass (%)	0.01	0.37	0.01	0.002	17.4	1.78	0.03	13.5	2.12	0.07	Bal.

(ISO) as a primary indication of the material's biocompatibility [18]. Additionally, there are *in vitro* tests capable of evaluating the mutagenic character of a material when used in contact with living cells. These are called genotoxicity tests. According to the ISO standard 10993 (part 3) [19], the genotoxicity of materials designed to get into contact with human tissues whatever in a temporary or permanent use must be considered. There is no information on the mutagenic character of PVD TiCN-coated implants in the literature.

The aim of this work was to investigate the corrosion behavior of TiCN-coated AISI 316 L stainless steel in Hanks' solution using electrochemical impedance spectroscopy and potentiodynamic polarization. The surface morphology of the samples was assessed using scanning electron microscopy (SEM). The primary *in vitro* biocompatibility of TiCN-coated 316 L stainless steel was performed by cytotoxicity and genotoxicity tests.

2. Experimental

2.1. Material

The chemical composition of the medical grade 316 L stainless steel used in this work is given in Table 1.

2.2. TiCN coating deposition

TiCN coatings were deposited using a HTC 1200 PVD unit manufactured by Hauzer Techno Coating Europe BV Venlo, The Netherlands. This machine uses four orthogonally mounted cathodes ($1000 \times 170 \times 14$ mm), which surround a three fold rotation substrate holder turntable. The cathodes are equipped with a cathodic arc deposition technique. Before deposition, specimens were cleaned in phosphoric acid, alkaline and detergent solution and deionized water in an ultrasonic cleaner system. Metallic ion etching was also performed to improve adhesion. Ionized metallic ions were accelerated from cathode to tolls biased in 1200 V. The deposition occurs in four steps: pump down and heating, metal ion etching, reactive deposition and cool down. The detailed process parameters are show in Table 2. The deposition rate was 0.8–1.0 μm/h. The resulting film thickness was approximately 2 μm. No interlayer was deposited between the substrate and the TiCN film.

2.3. Phase, crystallite size and residual stress analysis

X-ray diffraction (XRD) measurements were used to characterize the phases, crystallite size and residual stresses in the TiCN coating. The equipment used for phase and crystallite size analyses was a Rigaku diffractometer (Cu K_α). The mean crystallite size was estimated

by means of the linear fitting method [20]. Assuming that the overall broadening of XRD reflections is comprised of two components, grain size and microstrain, the identification of the individual contributions from mean crystallite size (D) and microstrain (ε) must be separated. The determination of D is based on Eq. (1).

$$\Delta(2\theta)\cos\theta = 2\varepsilon\sin\theta + 0.9\lambda / D \qquad (1)$$

where λ is the X-ray wavelenght and θ is the diffraction angle. The $\Delta(2\theta)\cos\theta$ was plotted against sinθ for the following XRD reflections (111), (200), (220), (311) and (422). The data falls on a straight line, with a slope of 2ε and an intercept of 0.9λ/D. Using λ = 0.154 nm for Cu Kα radiation the mean crystallite size of the TiCN coating was determined to be 22.3 nm.

Residual stress analysis was performed on TiCN (420) reflection at $2\theta \cong 108°$ using Cu tube and Ni filter with tilts in the range $\psi = \pm 30°$. The $\sin^2\psi$ method was used to evaluate the data [21]. This method is based on the determination of elastic strain in terms of the variation of the lattice spacings, d_ψ, of a selected diffraction plane inclined at an angle ψ in relation to the specimen surface. As the elastic stress normal to a free surface is zero, the interplanar spacings, d_n, of planes parallel to the specimen surface may be used as a reference for the strain free condition. The strains in planes inclined at an angle ψ in relation to the specimen surface may be expressed in terms of $\Delta d/d_n$, where $\Delta d = d_n - d_\psi$. The biaxial residual stress (σ) in a plane parallel to the surface of the TiCN film was calculated from the linear slope fitted to a plot of $\Delta d/d_n$ versus $\sin^2\psi$ by means of Eq. (2).

$$\frac{\Delta d}{d_n} = \sigma.\frac{(1-\nu)}{E}.\sin^2_\Psi \qquad (2)$$

In this equation E is the Young's modulus of the TiCN film and ν is its Poisson's ratio. The values for TiCN film were taken from literature as E = 332 GPa [22] e ν = 0,18 [23]. From this method compressive residual stresses of 5.08 GPa were determined in the film.

2.4. Electrochemical impedance spectroscopy (EIS)

The tests were performed at the open circuit potential, using a platinum wire as counter-electrode and a standard calomel electrode (SCE) as reference. The amplitude of the perturbation signal was 10 mV, the frequency range investigated was 100 kHz to 10 mHz with 6 points per decade using a frequency response analyzer (Solartron 1255) coupled to a potentiostat (EG&G 273A). The tests were performed at 37 °C in Hanks' solution (composition given in Table 3). The EIS diagrams were obtained after 1 and 28 days of immersion in the electrolyte. The results are given as Bode and Nyquist plots. The experimental data were fitted with equivalent circuits (ECs) using the Z_{view} software to give a more quantitative analysis of the EIS response.

2.5. Polarization measurements

For the polarization measurements the experimental set-up comprised a three-electrode arrangement with a platinum wire and

Table 2
Deposition parameters for TiCN films.

Steps	Steps conditions	Switch parameters	
Pump down and heating	–	5×10^{-5} mbar	450 °C
Metal ion etch	Substrate voltage 900–1200 V Arc current 140 A	5 min	450 °C
Reactive deposition	Substrate voltage 80 V	6×10^{-3} mbar	450eg
Arc current 140 A			
		$(8/1-N_2/C_2H_2)$	
Cool down	–	5×10^2 mbar$-N_2$	<200 °C

Table 3
Composition of Hanks' solution.

Component	Concentration (M)
NaCl	0.1369
KCl	0.0054
$MgSO_4.7H_2O$	0.0008
$CaCl_2.2H_2O$	0.0013
$Na_2HPO_4.2H_2O$	0.0003
KH_2PO_4	0.0004
$C_6H_{12}O_6.H_2O$	0.0050

a saturated calomel electrode (SCE) as counter and reference electrodes, respectively. A potentiostat/galvanostat EG&G 273A was used for the measurements. Potentiodynamic polarization curves were obtained after 28 days of immersion in Hanks' solution at 37 °C for both bare and TiCN-coated specimens, using a scanning rate of 1 mV s^{-1}. The potential range was from -0.8 V$_{ECS}$ to $+1,5$ V$_{ECS}$.

2.6. Scanning electron microscopy (SEM)

SEM-analyses were performed using a Philips XL30 microscope on TiCN-coated 316 L before immersion in Hanks' solution.

2.7. In vitro biocompatibility

The *in vitro* biocompatibity was performed with Chinese Hamster ovary cell line (CHO-k1). The cells were maintained in RPMI medium supplemented with antibiotics and antimicotic (100 units/mL penicillin, 100 µg/mL streptomycin and 0.025 µg/mL amphotericin), 2 mM glutamine, and 10% fetal bovine serum, at 37 °C in a humidified 5% CO_2 atmosphere until they reached confluence. For subculturing and for experiments, cells were harvested using 0.05% trypsin and 0.02% EDTA in phosphate-buffered solution, pH 7.4.

Bare 316 L and TiCN-coated 316 L were sterilized by heating and immersed in RPMI medium, using the ratio between the surface area and the volume of extraction vehicle of 1 cm^2/mL at 37 °C for 48 h. The extract was used to carry out the cytotoxicity and genotoxicity tests, as recommended by ISO 10993 parts 5 and 3 respectively [18,19].

Cytotoxicity test was performed in 96 well microplates seeded with 3000 cells per well and extracts dilutions from 100 to 6.25%. The microplates were incubated for 72 h at 37 °C in a humidified 5% CO_2 atmosphere. The cell viability was measured by adding 20 µL of MTS/PMS (20:1) solution and incubated for 2 h at 37 °C in the humidified 5% CO_2 incubator. The microplates were read in a spectrophotometer reader at 495 nm. The test was compared with a negative control of titanium and a positive control of phenol 0.3% in saline 0.9% solution. The Index of Cytotoxicity for 50% of cell viability (IC$_{50}$) was graphically estimated.

Genotoxicity test also known as the micronucleus test was performed in 6 well plates with and without the S9 metabolic activation system [24]. CHO-k1 cells were seeded at a concentration of 2×10^4 cell/well and incubated for 24 h at 37 °C in a humidified 5% CO_2 atmosphere. The culture media were removed from the plates and the cells were treated with the controls and extracts in the concentration of 100 and 30%. The test used cytochalasin B 3 µg/mL solution and were analyzed, after fixation and dying by Giemsa 5%, for cell frequency of mononucleate, binucleate and multinucleate. The total numbers of cells were used to determine the cell proliferation index (CPI). This test followed the OECD guideline number 487 [25].

2.7.1. Assay with S9 metabolic activation

The S9 metabolic activation mixture was added to the plates, with the analyzed extract and included cyclophosphamide (CPA) and benzopyrene (BZP), as positive control. The cultures were taken to the incubator for a 4 h exposure period. After the treatment period, the extracts were removed by aspiration and the cells were rinsed with phosphate buffer solution pH 7.4 and replenished with culture medium containing cytochalasin B 3 µg/mL. The cultures were then returned to the incubator for additional 20 h. After this period, the cultures were processed as subculture procedure as described below to prepare slides for analysis.

2.7.2. Assay without S9 metabolic activation

Plates containing the extract in the different concentrations and mitomycn C (MMC) and colchicine as control were incubated for 4 h

with the cells. After that, cytochalasin B solution was added to the wells at a final concentration of 3 µg/mL. The cultures were then returned to the incubator for a 20 h exposure period. At the end of incubation, the cultures were processed as subculture procedure as described below to prepare slides for analysis.

2.7.3. Slide preparation and analysis

The cell suspension was first washed with 5 mL of saline solution 0.9% (w/v) and after 5 min the cells were fixed by addition of 5 mL of methanol/acetic acid (3:1 v/v) for 5 min. The cells were treated with the fixative solution for more 3 times and finally resuspended by drawing and expelling with a Pasteur pipette, dropped onto wet clean glass slides on termostatized bath at 65 °C for 3 min and left air-dried. The slides were stained for 15 min with Giemsa 5%, rinsed with distilled water, coded and analyzed at an optical microscope with 400× of magnification. The mononucleate, binucleate and multinucleate cells were counted to determine the cell proliferation index (CPI) as shown in Eq. (3).

$$CPI = \frac{\text{no. mononucl. cells} \pm 2 \times \text{no. binucl. cells} \pm 3 \times \text{no. multinucl. cells}}{\text{Total number of cells}}$$

(3)

The binomial proportion was used for statistical analyses. An optical micrograpn of mono and binucleated cells is shown in Fig. 1.

3. Results and discussion

3.1. XRD measurements

The XRD pattern of TiCN coating is given in Fig. 2. The analysis revealed the presence of only the TiN phase in the film. Peaks of the AISI 316 L substrate (austenite Fe-γ) are also clearly seen [26]. There is a strong orientation in the TiN (111) reflection. According to Schneider et al. [27] the plane (111) orientation is favored during the growing of the film as it is the most densely packed plane in the film structure. In addition, this orientation favors the growing of a columnar layer [28]. Consequently, the film would be more prone to corrosion in an aqueous electrolyte, as its columnar structure facilitates the penetration of aggressive ions through the coating.
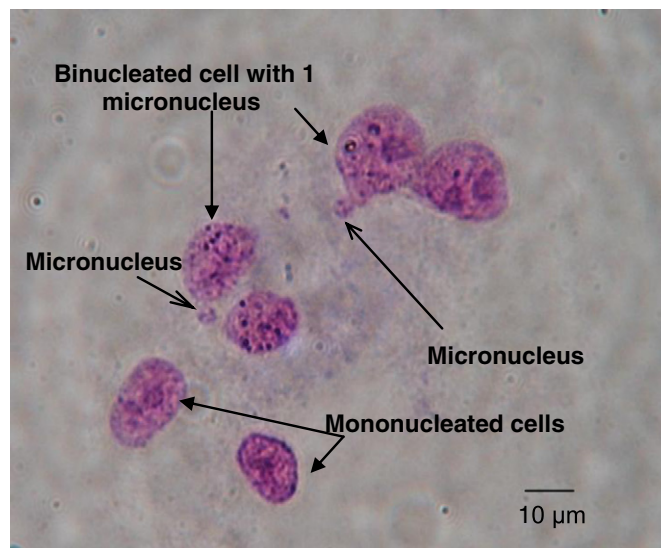

Fig. 1. Optical microscope photo showing examples of mono and binucleated cells counted for the determination of the CPI (400×).
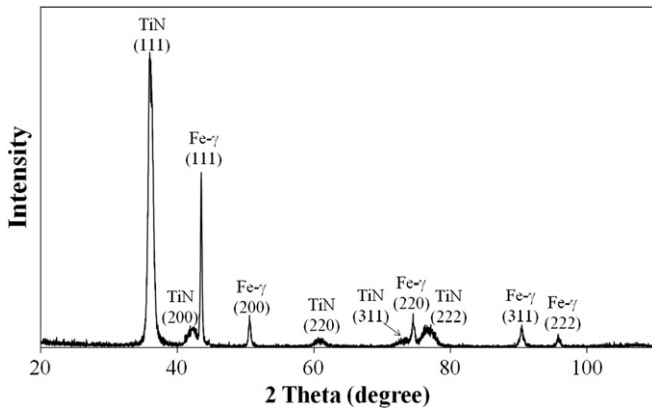
Fig. 2. XRD patterns of the TiCN film.

3.2. Coating morphology

The surface morphology of TiCN film is shown in Fig. 3. Typical features of PVD coatings like pinholes and macros are clearly seen on the specimen surface. These defects are intrinsic to PVD processes [29].

3.3. Electrochemical tests

Bode (phase angle) plots of bare and TiCN-coated 316 L after 1 and 28 days of immersion in Hanks' solution at 37 °C are shown in Fig. 4.

The Bode plot of Fig. 4 shows that bare 316 L was highly capacitive after 1 day of immersion. This behavior is typical of passive metals and has been identified by other authors for 316 L stainless steel [30]. After 28 days the material remained passive but there are two time constants. The first, characterized by a shoulder in the frequency range 10^2–10^3 Hz, may be ascribed to the electrochemical response of the passive layer on the 316 L surface. Considering that the passive layer is not perfect and presents some intrinsic defects that may be a pathway to the penetration of the electrolyte the physical meaning of the second time constant at lower frequencies is considered to be due to the response of the metallic substrate on the base of the passive layer defects. It is important to realize the stable character of the 316 L along the whole period of immersion which indicates its high corrosion resistance in the conditions of the test.

The electrochemical behavior of TiCN-coated 316 L differs from that of the bare material. After the first day of immersion the phase diagrams presented a very similar behavior in the high frequency region. However, when one considers the medium to low frequencies

Fig. 3. SEM micrograph of TiCN-coated 316 L specimen prior to immersion in Hanks' solution.
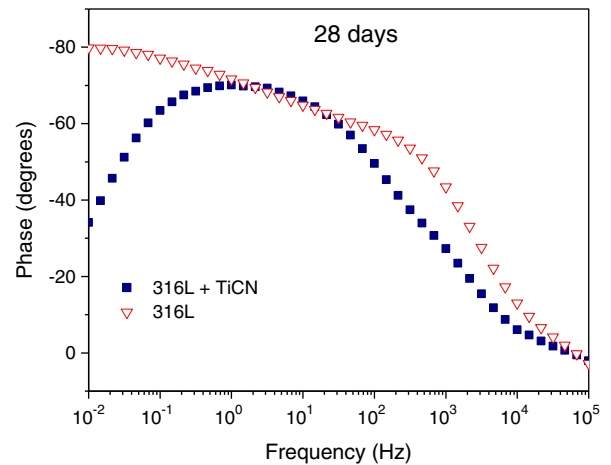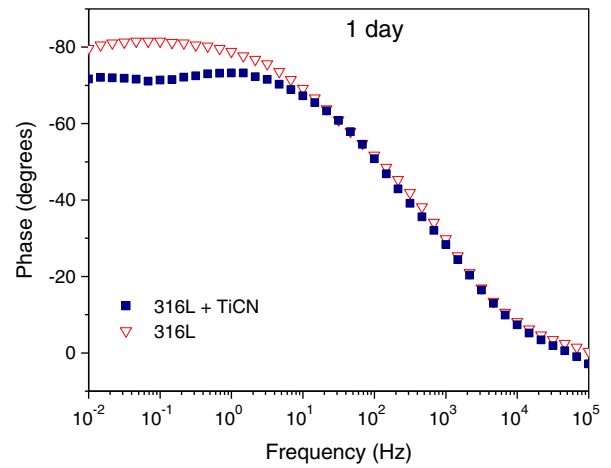

Fig. 4. Bode plots of bare and TiCN-coated 316 L after 1 and 28 days of immersion in Hanks' solution at 37 °C.

the coated specimen is less capacitive than the bare one. This effect is very possibly related to the TiCN film morphology. As shown in Fig. 3, the film surface presents pinholes that alloy the penetration of the electrolyte. This situation may lead to a slow dissolution of the metallic substrate on the base of the coating defects. The sharp decrease of phase angle at low frequencies after 28 days of immersion is an indication of this mechanism.

Nyquist plots of bare and TiCN-coated 316 L after 1 and 28 days of immersion in Hanks' solution at 37 °C are shown in Fig. 5.

As shown in Fig. 5 both bare and TiCN-coated 316 L the impedance values of bare 316 L is higher than those of the TiCN-coated material either after 1 or 28 days of immersion in the electrolyte. The Nyquist plots are characterized by a capacitive loop whose radius diminishes from 1 to 28 days. The impedance decrease is sharper for the TiCN-coated specimen, confirming the results showed on Fig. 4. As discussed earlier, the deterioration of the corrosion behavior of the TiCN-coated specimen may be related to the penetration of the electrolyte through the coating defects.

The equivalent electric circuits used to fit the experimental data of Figs. 4 and 5 are shown in Fig. 6. The capacitive behavior was simulated using constant phase elements (CPEs) instead of pure capacitors accounting for the inhomogeneities of the material surfaces [31]. The EIS response of the uncoated 316 L stainless steel was simulated with the circuit of Fig. 5a. This circuit was proposed by Pan et al. [32] to simulate the electrochemical behavior of titanium in saline solutions. It may be interpreted as an electrical representation of an oxide layer that presents a duplex character, i.e., it consists of an inner compact layer that acts as a barrier against the penetration of
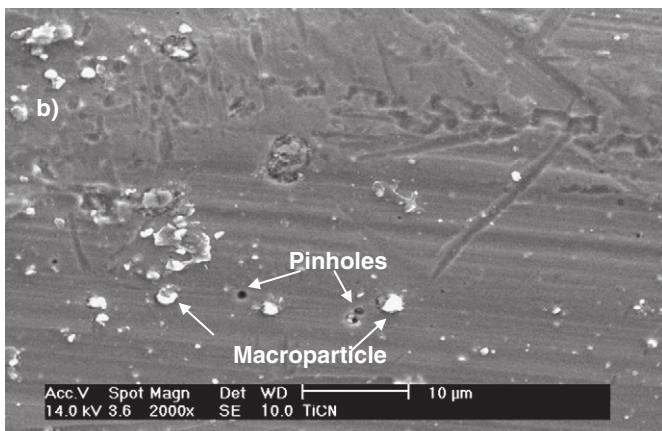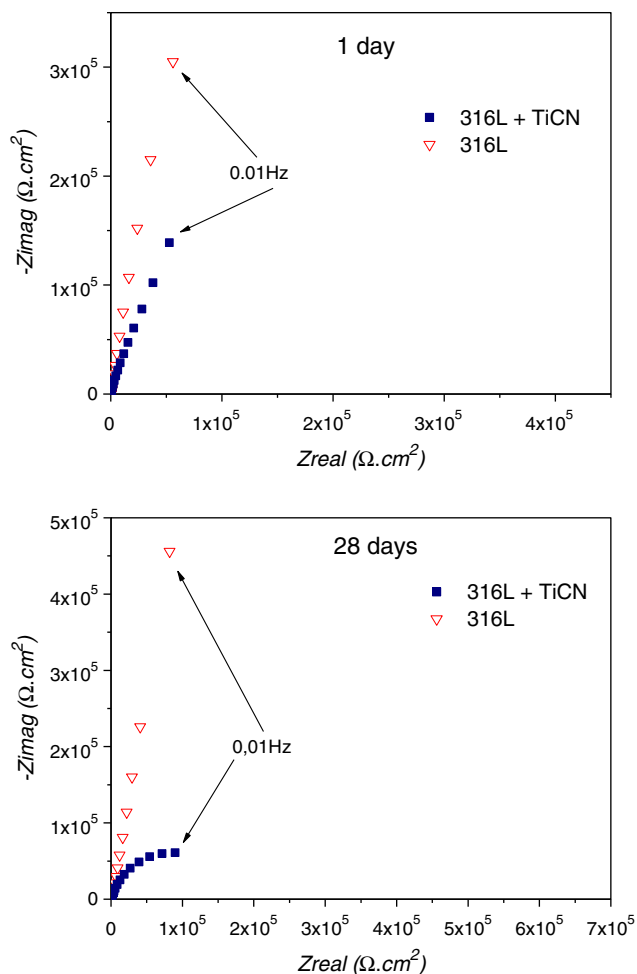
Fig. 5. Nyquist plots of bare and TiCN-coated 316 L after 1 and 28 days of immersion in Hanks' solution at 37 °C.

the electrolyte and an external porous layer that is permeable to the aggressive chemical species in the electrolyte. According to the literature the passive layer on the stainless steels also present a duplex character [33–35]. The external layer, in this case, is composed mainly of iron oxides while the internal barrier layer consists of chromium oxide. This behavior is extensively documented through the study of the semiconducting properties of the passive films formed on stainless steels using the Mott–Schottky approach and
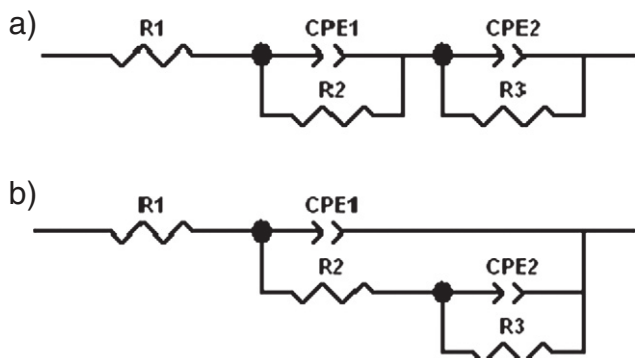

Fig. 6. Equivalent electric circuits used to fit the experimental EIS data of Figs. 3 and 4: a) uncoated 316 L; b) TiCN-coated 316 L.

surface chemical analysis such as Auger electron spectroscopy (AES) or X-ray photoelectrons spectroscopy (XPS) [36,37]. Indeed, Rondelli et al. [38] confirmed the validity of the circuit in Fig. 6a to model the EIS experimental data of a nickel-free stainless steel in physiological solutions. So, in this circuit R_1 is the electrolyte resistance, while R_2-CPE_1 and R_3-CPE_2 are the resistances and constant phase elements of the outer and inner layers, respectively. The corrosion resistance would be due to the chromium-rich inner film. The results of the fitting procedure are summarized in Table 4. The chromium-rich inner film is the layer mainly responsible for the corrosion resistance.

For the TiCN-coated 316 L stainless steel the circuit of Fig. 6b produced the best fitting results. This equivalent circuit is typical of a metallic material with a defective coating layer [39–41]. The defects of the TiCN film are clearly observed in Fig. 3. The parameter R_1 is the electrolyte resistance. R_2 and Q_1 are the resistance and capacitance the TiCN film, modeling the electrochemical behavior at high frequencies. R_3 and Q_2 are associated, respectively, with the resistance and capacitance of the passive film at the base of the coating defects and are related to corrosion processes at lower frequencies.

From Table 4 it is noteworthy that R_2 for the uncoated stainless steel increases with immersion time and Q_1 (the capacitance of the CPE_1 element) was reduced. The value of the resistive element R_3, used to model the resistance of the chromium-rich inner layer, diminished with the immersion time while its capacitance Q_2 presented a small increase. Admitting that the 316 L passive film consists of an inner chromium-rich compact layer and an outer porous iron-rich layer, the evolution of the electrochemical behavior related to the interface passive layer/electrolyte may be given as follows. During the initial period of immersion the electrolyte penetrates through the porous external layer of the passive film. With the elapsed time, this layer is likely to thicken which, in turn, would reflect in an increase of the capacitance Q_1. Ge et al. [42], investigating the EIS response of 316 stainless steel in simulated cooling water, related variations of the parameters Q_2 and R_3 to modifications of the compactness of the passive film on the stainless steel surface. Thus, an increase of the resistance and a reduction of the capacitance would indicate the formation of a less defective oxide layer with the immersion time. As shown in Table 4, the variations of R_3 and Q_2 are opposite to this tendency, suggesting that the inner layer became more conductive with the immersion time. Such effect could result from the penetration of the chloride ions in the Hanks' solution through the external iron-rich layer. These ions would reach the inner compact layer of the passive film, leading to an acceleration of the charge transfer reactions. This, in turn, would lead to the decrease of the resistance R_3 and the increase of the capacitance Q_2.

For the TiCN-coated material the values of R_3 strongly decreased from 1 to 28 days of immersion while R_2 was little affected. The TiCN coating is relatively inert which would explain the parameters R_2 and Q_1. Li et al. [29] stated that due to the inert character of a TiN film the corrosion behavior of a PVD coated stainless steel was governed by the underlying metal at the base of the film defects. As TiCN is also inert the same supposition may be done here. The results in Table 4

Table 4
Values for the elements of the equivalent circuits shown in Fig. 5a and b. for uncoated and TiCN-coated 316 L stainless steel in Hanks' solution at 37 °C after 1 and 28 days of immersion.

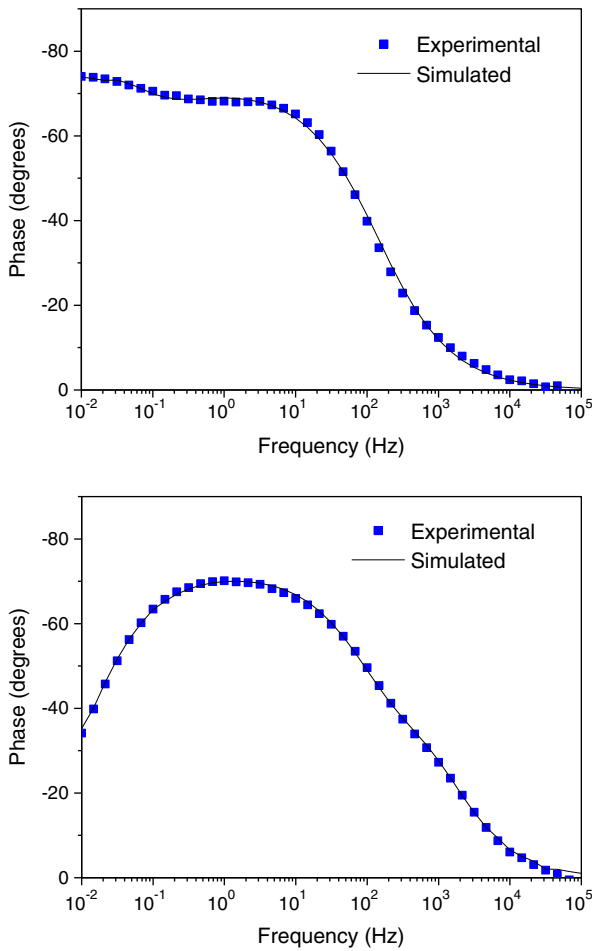| Element	316 L		TiCN-coated 316 L	
	1 day	28 days	1 day	28 days
R_1 (Ω cm^2)	57.6	53.3	30.9	39.5
Q_1 (cm^{-2} s$^{-n}\Omega$) 10^{-4}	1.26	0.78	0.31	0.20
R_2 (Ω cm^2)	5870	17556	164	128
Q_2 (cm^{-2} s$^{-n}\Omega$) 10^{-5}	4.48	6.73	2.33	2.93
R_3 (kΩ cm^2)	2250	783	1870	168

Fig. 7. Experimental and fitted data for: (a) uncoated and (b) TiCN-coated 316 L stainless after 28 of immersion in Hanks' solution at 37 °C.

corroborate this assumption. Indeed, the Bode and Nyquist plots of Figs. 4 and 5 show a strong decrease of the impedance with the time of immersion at low frequencies. This time constant is associated with the response of the 316 L passive film at the base of the defects in the TiCN film. The resistance of the passive layer (R_3) showed a ten-fold decrease from 1 to 28 days of immersion. It is likely, then, that the penetration of the electrolyte through the coatings defects led to the

deterioration of the overall protective character of the coating material. Additionally, the defects may act as occluded cells, presenting a catalytic effect on the corrosion process of the material and leading to localized attack at the coating/substrate interface [39].

Fig. 7 shows the comparison between the experimental and fitted data of the Bode diagrams for 28 days of immersion presented in Fig. 4. The quality and adequacy of the fitting procedure are clearly seen. A physical model for the EIS response of uncoated and TiCN-coated 316 L stainless steel is given in Fig. 8.

The model for the uncoated 316 L outlines the duplex character of its passive film, with the inner compact chromiun-rich layer and the outer porous iron-rich layer. The electrolyte penetrated through the outer layer during the initial periods of immersion. Subsequently, the outer layer thickens leading to an increase of R_2 and the reduction of Q_1. The increase of Q_2 and decrease of R_3 with the elapsed time would be associated with the attack of the inner layer due to the aggressive species that penetrates through the defects and porous of the outer layer. The model of the TiCN-coated material is based on the presence of the intrinsic defects typical of PVD processes which were shown in the SEM micrograph of Fig. 3. The permeable defects act as pathways to the penetration of the electrolyte that reaches the metal substrate. This exposure accounts for the significant reduction of R_3 with the immersion time. The decrease of the impedance values at low frequencies shown in the Nyquist plots of Fig. 5 confirms the suitability of this model.

Potentiodynamic polarization curves of bare and TiCN-coated 316 L after 28 days of immersion in Hanks' solution at 37 °C are shown in Fig. 9. The presence of the TiCN coating shifted the corrosion potential by only 50 mV$_{SCE}$ toward more positive values. However, the corrosion current density of the bare specimen is slightly lower than that of the TiCN-coated one (0.35 μA cm^{-2} for the uncoated specimen and 0.49 μA cm^{-2} for the TiCN-coated one). The cathodic part of the curves are very similar for both specimens. On the other hand, in the anodic region there are clear differences between the two specimens. The bare specimen presents a passive range between −200 mV$_{SCE}$ to +200 mV$_{SCE}$. The sharp increase of the current density at this potential indicated the breakdown of passivity and the onset of pitting corrosion. For the TiCN-coated one there is a continuous and slow increase of the current density with the potential. This behavior resembles that of active materials. The sharp increase of current density near +1200 mV$_{SCE}$ is probably due to the oxygen evolution reaction. While some authors [5,43] reported that TiCN films are effective to enhance the corrosion properties of metallic substrates, Marin et al. [44] have also found that PVD TiCN films did not improve the corrosion resistance of a high speed steel. The coating morphology
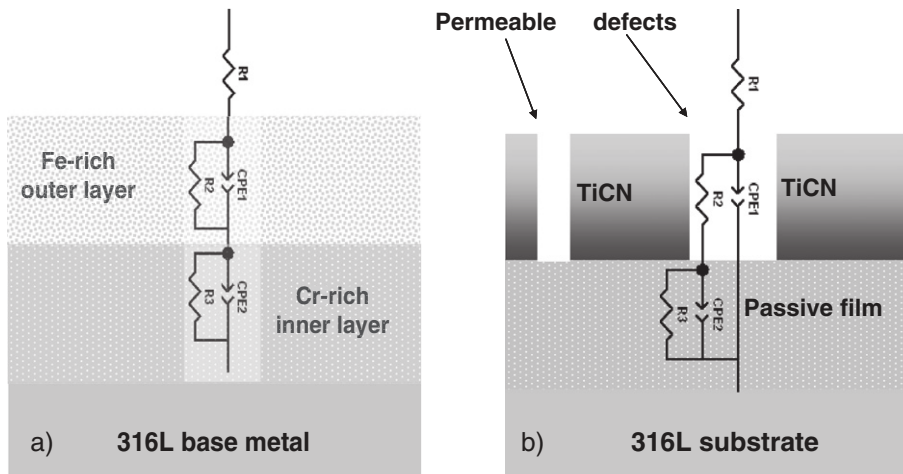

Fig. 8. Physical models of uncoated and TiCN-coated 316 L stainless steel based on the EIS results.
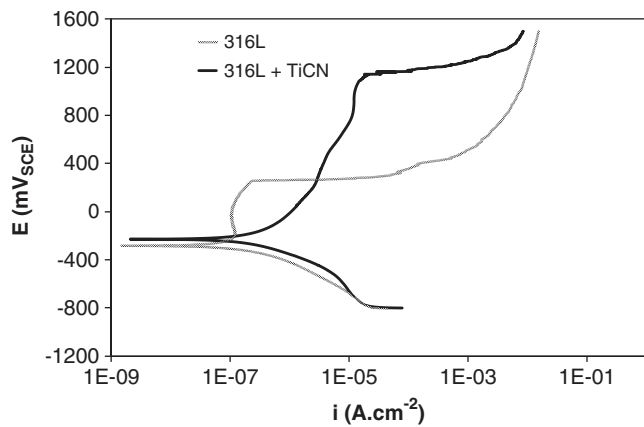
Fig. 9. Potentiodynamic polarization curves of bare and TiCN-coated 316 L after 28 days of immersion in Hanks' solution at 37 °C.

is the key factor that leads to a desirable corrosion resistance improvement or a deleterious poorly protective situation. The potentiodynamic curves of Fig. 9 show that the TiCN film did not provide a suitable protection to the 316 L substrate. This finding confirms the EIS results shown in Figs. 4 and 5. The incipient protective character imparted by the TiCN layer is directly related to the presence of permeable defects in the film. However, despite the little effect on corrosion potential and corrosion current density, the TiCN coating did not present a sharp current density increase up to +1200 mVSCE. Thus, it does have a positive effect on the pitting corrosion resistance in comparison with the bare material. Deposition process parameters such as substrate bias, temperature and current density may be controlled in order to obtain a more compact, denser and corrosion resistant PVD layer [45,46]. PVD multilayered coatings are a recent architecture that has been shown to increase the corrosion resistance of coated metals [47,48]. Multilayered coatings give rise to a longer diffusion path to the electrolyte, thus reducing the corrosion rate of the metallic substrate. Furthermore, the probability that a defect in the film reaches the substrate is also diminished.

3.4. In vitro biocompatibility

The cytotoxicity assay of bare 316 L and TiCN-coated 316 L was carried out by a colorimetric method based on the quantitative assessment of surviving viable cells upon exposure to the toxic agent. The amount of MTS, the marker of cell viability, taken up by the population of cells, is directly proportional to the number of viable cells in the culture [13].

The cell viability determinations are shown in Fig. 10. The materials tested did not present any cytotoxic effect similar to the
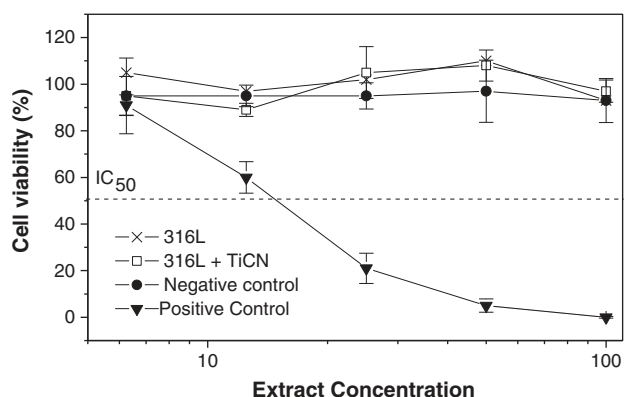
negative control (IC$_{50}$ >100) showing their harmless character. To confirm the reliability of the method the positive control showed a cytotoxic effect over the cells (IC$_{50}$ = 15). The cytotoxicity test in the biological evaluation is a toxicological screening test that can predict the biocompatibility of 316 L stainless steel wherever TiCN-coated or not. This is a primary indication of the suitability of TiCN-coated 316 L stainless steel for biomedical applications.

The genotoxicity results of bare 316 L and TiCN-coated 316 L are shown in Fig. 11. In the presence of the metabolic activation system S9 the CPI values of the TiCN extracts, either 100% or 33% concentrated, are very close to the cell medium. The positive control (benzopyrene) presented lower CPI value confirming its mutagenic character. For the test without the metabolic activation system S9 the CPI values for the TiCN extracts are much higher than those presented by the positive controls (mitomycin C and colchicine). The CPI values of TiCN were also higher than those of positive control (benzopyrene) in the test with S9. These results show that TiCN film was not genotoxic according to the methodology employed in this work. Allied with the cytotoxicity test results these data indicate the biocompatibility of titanium carbonitride and its potential use for biomedical applications.

4. Conclusions

The surface defects on TiCN films strongly influenced the corrosion resistance of AISI 316 L stainless steel. Apparently the bare 316 L stainless was more stable in Hanks' solution when compared to the TiCN-coated specimen. The penetration of the electrolyte through pinholes on the TiCN film led to the decrease of impedance values observed on the Nyquist plots along the immersion time. The TiCN-coated specimen did not present a typical passive behavior. However, the current densities are low.

Both cytotoxicity and genotoxicity tests revealed the biocompatible nature of the TiCN film which is a primary indication of its potential use as a coating for biomedical devices. Despite the suitability of the biological response, there is a need to further improve the electrochemical behavior of the PVD layer in order to achieve a consistent performance in real implant devices. It has to be emphasized that the results reported here were obtained under static conditions of immersion. Nevertheless, TiCN films are envisaged as coatings for femoral heads in hip replacement, for instance. In theses cases, the high hardness, wear and fatigue resistances of this material would be of prime interest for a successful application. If, under static conditions, the corrosion resistance is not effective, when the mechanical factors such as wear and fatigue are present, the damage to the PVD film should be dangerously sharper. So, a careful control of
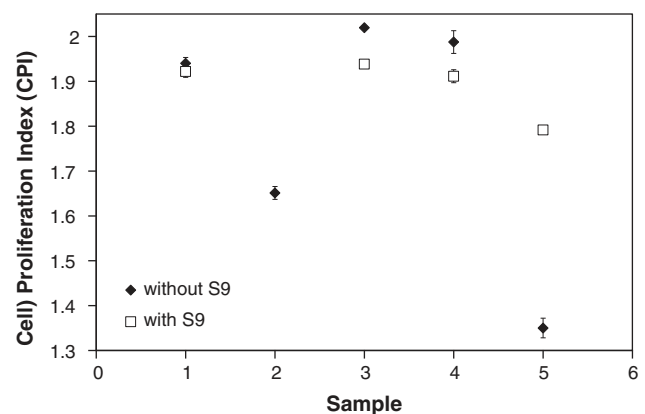

Fig. 10. Cell viability curves of bare and TiCN-coated 316 L stainless steel.

Fig. 11. Graphic representation of the genotoxicity test results with the cell proliferation index (CPI ± δ), with S9 and without S9. Numbered samples are: 1 — culture medium (control); 2 — positive control (mitomycin C); 3 — extract (100%); 4 — extract (33%); and 5 — positive controls (♦) colchicine and (□) benzopyrene.

the PVD parameters is essential to obtain a coating morphology that avoid the formation of permeable defects that may act as preferential sites to the penetration of aggressive ions present in the human body fluid.

Acknowledgements

References

[1] S. Kannan, A. Balamurugan, S. Rajeswari, Mater. Lett. 57 (2003) 2382–2389.
[2] S. Xulin, A. Ito, T. Tateishi, A. Hoshino, J. Biomed. Mat. Res. 34 (1997) 9–14.
[3] I. Gurappa, Mater. Charact. 49 (2002) 73–79.
[4] H.-P. Feng, C.-H. Hsu, J.-K. Lu, Y.-H. Shy, Mater. Sci. Eng. A 347 (2003) 123–129.
[5] S. Surviliene, S. Bellozor, M. Kurtinaitiene, V.A. Safonov, Surf. Coat. Technol. 176 (2004) 193–201.
[6] A.P. Serro, C. Completo, R. Colaço, F. dos Santos, C.L. da Silva, J.M.S. Cabral, H. Araújo, E. Pires, B. Saramago, Surf. Coat. Technol. 203 (2009) 3701–3707.
[7] M.P. Gispert, A.P. Serro, R. Colaço, E. Pires, B. Saramago, Wear 263 (2007) 1060–1065.
[8] T. Liskiewicz, S. Fouvry, B. Wendler, Wear 259 (2005) 835–841.
[9] T. Polcar, R. Novák, P. Siroky, Wear 260 (2006) 40–49.
[10] L.F. Senna, C.A. Achete, T. Hirsch, F.L. Freire Jr., Surf. Coat. Technol. 94–95 (1997) 390–397.
[11] W. Precht, E. Lunarska, A. Czyzniewski, M. Pancielejko, W. Walkowiak, Vacuum 47 (1996) 867–869.
[12] N. Donnelly, M. McConnell, D.P. Dowling, J.D. O'Mahony, Mater. Sci. Forum 325–326 (2000) 141–146.
[13] F. Hollstein, P. Louda, Surf. Coat. Technol. 120–121 (1999) 672–681.
[14] D. Mattox, Metal Finishing 100 (2002) 396–408.
[15] B.S. Yilbas, A.Z. Sahin, Z. Ahmad, B.J.A. Aleem, Corr. Sci. 37 (1995) 1627–1636.
[16] D. Yang, C. Liu, X. Liu, M. Qi, G. Lin, Curr. Appl. Phys. 5 (2005) 417–421.
[17] R.M. Souto, H. Alanyali, Corr. Sci. 42 (2000) 2201–2211.
[18] International Organization for Standardization, ISO 10993-5; Biological testing of medical and dental materials devices — part 5. Tests for cytotoxicity: in vitro methods, Switzerland, 1992.
[19] International Organization for Standardization, ISO 10993-3; Biological testing of medical and dental materials devices — part 3. Tests for genotoxicity and reproductive toxicity. Switzerland, 1992.
[20] J.W. Jeffery, Methods in X-ray Crystallography, Academic Press, London and New York, 1971 83pp.
[21] I.C. Noyan, J.B. Cohen, Residual Stress Measurement by Diffraction and Interpretation, Springer-Verlag, New York, 1987.
[22] R.A. Antunes, Thesis, University of São Paulo, 2006.
[23] T.-H. Fang, S.-H. Jian, D.-R. Chuu, Appl. Surf. Sci. 228 (2004) 365–372.
[24] M.L. Garriott, J.B. Phelps, W.P. Hoffman, Mut. Res. 517 (2002) 123–134.
[25] Organization for Economic Co-operation and Development. OECD Guideline for Testing of Chemicals. No. 487: In vitro Micronucleus Test. Available at www.oecd.org/. Accessed January 12, 2010
[26] JCPDS, Powder Diffraction File, International Center for Powder Diffraction Data, Swarthmore, PA, 1993, Cards 87-0632, 33-0397.
[27] J.M. Schneider, A. Voevodin, C. Rebholz, A. Matthews, J.H.C. Hogg, D.B. Lewis, M. Ives, Surf. Coat. Technol. 74–75 (1995) 312–319.
[28] D. Yang, C. Liu, X. Liu, M. Qi, G. Lin, Curr. Appl. Phys. 5 (2005) 417–421.
[29] Y. Li, L. Qu, F. Wang, Corr. Sci. 45 (2003) 1367–1381.
[30] F.J. Pérez, M.P. Hierro, C. Gómez, L. Martínez, P.G. Viguri, Surf. Coat. Technol. 151 (2002) 250–259.
[31] C. Liu, Q. Bi, A. Leyland, A. Matthews, Corr. Sci. 45 (2003) 1243–1256.
[32] J. Pan, C. Leygraf, D. Thierry, A.M. Ektessabi, J. Biomed. Mater. Res. 35 (1997) 309–318.
[33] N. Hakiki, S. Baudin, B. Rondot, M. da Cunha Belo, Corr. Sci. 37 (1995) 1809–1822.
[34] M.F. Montemor, M.G.S. Ferreira, N.E. Hakiki, M. da Cunha Belo, Corr. Sci. 42 (2000) 1635–1650.
[35] M. da Cunha Belo, M. Walls, N.E. Hakiki, J. Corset, E. Picquenard, G. Sagon, D. Nöel, Corr. Sci. 40 (1998) 447–463.
[36] M. da Cunha Belo, B. Rondot, C. Compere, M.F. Montemor, A.M.P. Simões, M.G.S. Ferreira, Corr. Sci. 40 (1998) 481–494.
[37] M.J. Carmezim, A.M. Simões, M.F. Montemor, M. da Cunha Belo, Corr. Sci. 47 (2005) 581–591.
[38] G. Rondelli, P. Torricelli, M. Fini, R. Giardino, Biomaterials 26 (2005) 739–744.
[39] C. Liu, A. Leyland, S. Lyon, A. Matthews, Surf. Coat. Technol. 76–77 (1995) 615–622.
[40] F. Vacandio, Y. Massiani, P. Gergaud, O. Thomas, Thin Solid Films 359 (2000) 221–227.
[41] D.K. Merl, P. Panjan, M. Cekada, M. Macek, Electrochim. Acta 49 (2004) 1527–1533.
[42] H.-H. Ge, G.-D. Zhou, W.-Q. Wu, Appl. Surf. Sci. 211 (2003) 321–334.
[43] Y. Cheng, Y.F. Zheng, Surf. Coat. Technol. 201 (2007) 4909–4912.
[44] E. Marin, L. Guzman, A. Lanzutti, L. Fedrizzi, M. Saikkonen, Electrochem. Commun. 11 (2009) 2060–2063.
[45] A.S. Korhonen, Vacuum 45 (1994) 1031–1034.
[46] P. Gröning, S. Novak, L. Schlapbach, Appl. Surf. Sci. 62 (1992) 209–216.
[47] C. Liu, P.K. Chu, G. Lin, D. Yang, Corr. Sci. 49 (2007) 3783–3796.
[48] R. Bayon, A. Igartua, X. Fernández, R. Martínez, R.J. Rodríguez, J.A. García, A. De Frutos, M.A. Arenas, J. De Damborenea, Tribol. Int. 42 (2009) 591–599.